International Communications in Heat and Mass Transfer 36 (2009) 996–1001

Contents lists available at ScienceDirect

International Communications in Heat and Mass Transfer

journal homepage: www.elsevier.com/locate/ichmt

Numerical simulation of turbulent combustion in porous materials ☆

Marcelo J.S. de Lemos

Departamento de Energia, IEME, Instituto Tecnológico de Aeronáutica, ITA, 12228-900, São José dos Campos, SP, Brazil

ARTICLE INFO

Available online 6 August 2009

Keywords:
Porous burner
Combustion
Radiation
Ceramic foam
Turbulence modeling

ABSTRACT

This paper presents one-dimensional simulations of combustion of an air/methane mixture in porous materials using a model that explicitly considers the intra-pore levels of turbulent kinetic energy. Transport equations are written in their time-and-volume-averaged form and a volume-based statistical turbulence model is applied to simulate turbulence generation due to the porous matrix. Four different thermo-mechanical models are compared, namely Laminar, Laminar with Radiation Transport, Turbulent, Turbulent with Radiation Transport. Combustion is modeled via a unique simple closure. Preliminary testing results indicate that a substantially different temperature distribution is obtained depending on the model used. In addition, for high excess air peak gas temperature is reduced and the flame front moves towards the exit of the burner. Also, increasing the inlet flow rate for stoichiometric mixture pushes the flame out of the porous material.

1. Introduction

Combustion in inert porous media has been extensively investigated due to the many engineering applications and demand for developing high-efficiency power production devices. The growing use of efficient radiant burners can be encountered in the power and process industries and, as such, proper mathematical models of flow, heat and mass transfer in porous media under combustion can benefit the development of such engineering equipment.

Accordingly, the advantages of having a combustion process inside an inert porous matrix are today well documented in the literature [1–8], including a recent review on lean-combustion porous burners [9]. Hsu et al. [10] points out some of its benefits including higher burning speed and volumetric energy release rates, higher combustion stability and the ability to burn gases of a low energy content. Driven by this motivation, the effects on porous ceramics inserts have been investigated in Peard et al. [11], among others.

Turbulence modeling of combustion within inert porous media has been conducted by Lim and Matthews [12] on the basis of an extension of the standard k–ε model of Jones and Launder [13]. Work on direct simulation of laminar in premixed flames, for the case when the porous dimension is of the order of the flame thickness, has also been reported in Sahraoui and Kaviany [14].

Further, non-reactive turbulence flow in porous media has been the subject of several studies [15–17], including many applications such as flow though porous baffles [18], channels with porous inserts [19] and buoyant flows [20]. In such line of work, intra-pore turbulence is accounted for in all transport equations, but only non-reactive flow has been previously investigated in [15–20].

Motivated by the foregoing, this paper extends the previous work on turbulence modeling in porous media to include simulation of reactive flows. Computations are carried out for inert porous material considering one-dimensional turbulent flow and a two-energy equation model.

In addition, four different thermo-mechanical models are here compared, namely Laminar Flow, Laminar Flow with Radiation Transport, Turbulent Flow and Turbulent Flow with Radiation Transport, being the last two models derived from the work in [15–20]. As such, this contribution compares the effects of radiation and turbulence in smoothing temperature distributions within porous burners.

2. Mathematical model

As mentioned, two of the thermo-mechanical models here employed, involving turbulent flow with and without radiation transport, are based on the "double-decomposition" concept [15,16], which has been also described in detail in a book [17]. In that work, transport equations are volume-averaged according to the Volume Averaging Theorem [21–23] in addition to using time decomposition of flow variables followed by standard time-averaging procedure for treating turbulence.

As the entire equation set is already fully available in the open literature, these equations will be just reproduced here and details about their derivations can be obtained in the aforementioned references. Essentially, in all the above-mentioned work the flow variables are decomposed in a volume mean and a deviation (classical porous media analysis) in addition of being also decomposed in a time-mean and a fluctuation (classical turbulent flow treatment).

☆ Communicated by W.J. Minkowycz.
E-mail address: delemos@ita.br.

0735-1933/$ – see front matter © 2009 Elsevier Ltd. All rights reserved.
doi:10.1016/j.icheatmasstransfer.2009.07.006

Nomenclature

Latin characters

A	Pre-exponential factor
c_F	Forchheimer coefficient
c_p	Specific heat
$D=\lfloor\nabla\mathbf{u}+(\nabla\mathbf{u})^T\rfloor/2$	Deformation rate tensor
D_ℓ	Diffusion coefficient of species ℓ
D_{diff}	Macroscopic diffusion coefficient
D_{disp}	Dispersion tensor due to dispersion
$D_{disp,t}$	Dispersion tensor due to turbulene
f_2	Damping function
f_μ	Damping function
D_{eff}	Effective dispersion
K	Permeability
k_f	Fluid thermal conductivity
k_s	Solid thermal conductivity
$\mathbf{K}_{eff}$	Effective Conductivity tensor
m_ℓ	Mass fraction of species ℓ
Pr	Prandtl number
S_{fu}	Rate of fuel consumption
T	Temperature
$\mathbf{u}$	Microscopic velocity
$\mathbf{u}_D$	Darcy or superficial velocity (volume average of $\mathbf{u}$)

Greek characters

α	Thermal diffusivity
β_r	Extinction coefficient
ΔV	Representative elementary volume
ΔV_f	Fluid volume inside ΔV
ΔH	Heat of combustion
μ	Dynamic viscosity
ν	Kinematic viscosity
ρ	Density
ϕ	$\phi={}^{\Delta V_f}/_{\Delta V}$, Porosity
Ψ	Excess air-to-fuel ratio

Special characters

φ	General variable
$\langle\varphi\rangle^i$	Intrinsic average
$\langle\varphi\rangle^v$	Volume average
${}^i\varphi$	Spatial deviation
$\overline{\varphi}$	Time average
$\lvert\varphi\rvert$	Absolute value (Abs)
$\boldsymbol{\varphi}$	Vetorial general variable
$(\ )_{s,f}$	solid/fluid
$(\ )_{eff}$	Effective value, $\phi\varphi_f+(1-\phi)\varphi_s$
$(\ )_\phi$	Macroscopic value

Because mathematical details and proofs of such concept are available in a number of papers in the literature, they are not repeated here, as already noted. These final equations in their steady-state form are the following.

2.1. Macroscopic continuity equation

$$\nabla\cdot\rho\overline{\mathbf{u}}_D=0 \tag{1}$$

where, $\overline{\mathbf{u}}_D$ is the average surface velocity (also known as seepage, superficial, filter or Darcy velocity) and ρ is the fluid density. Eq. (1) represents the macroscopic continuity equation for the gas.

2.2. Macroscopic momentum equation

$$\rho\nabla\cdot\left(\frac{\overline{\mathbf{u}}_D\overline{\mathbf{u}}_D}{\phi}\right)=-\nabla(\phi\langle\overline{p}\rangle^i)+\mu\nabla^2\overline{\mathbf{u}}_D+\nabla\cdot(-\rho\phi\langle\overline{\mathbf{u}'\mathbf{u}'}\rangle^i)+\phi\rho\mathbf{g}-\left[\frac{\mu\phi}{K}\overline{\mathbf{u}}_D+\frac{c_F\phi\rho|\overline{\mathbf{u}}_D|\overline{\mathbf{u}}_D}{\sqrt{K}}\right] \tag{2}$$

where the last two terms in Eq. (2), represent the Darcy and Forchheimer contributions. The symbol K is the porous medium permeability, $c_F=0.55$ is the form drag coefficient, $\langle p\rangle^i$ is the intrinsic (fluid phase averaged) pressure of the fluid, μ represents the fluid viscosity and ϕ is the porosity of the porous medium.

Turbulence is handled via a macroscopic k–ε model given by,

$$\rho\nabla\cdot(\overline{\mathbf{u}}_D\langle k\rangle^i)=\nabla\cdot\left[\left(\mu+\frac{\mu_{t_\phi}}{\sigma_k}\right)\nabla(\phi\langle k\rangle^i)\right]-\rho\langle\overline{\mathbf{u}'\mathbf{u}'}\rangle^i:\nabla\overline{\mathbf{u}}_D+c_k\rho\frac{\phi\langle k\rangle^i|\overline{\mathbf{u}}_D|}{\sqrt{K}}-\rho\phi\langle\varepsilon\rangle^i \tag{3}$$

$$\rho\nabla\cdot(\overline{\mathbf{u}}_D\langle\varepsilon\rangle^i)=\nabla\cdot\left[\left(\mu+\frac{\mu_{t_\phi}}{\sigma_\varepsilon}\right)\nabla(\phi\langle\varepsilon\rangle^i)\right]+c_1(-\rho\langle\overline{\mathbf{u}'\mathbf{u}'}\rangle^i:\nabla\overline{\mathbf{u}}_D)\frac{\langle\varepsilon\rangle^i}{\langle k\rangle^i}+c_2c_k\rho\frac{\phi\langle\varepsilon\rangle^i|\overline{\mathbf{u}}_D|}{\sqrt{K}}-c_2\rho\phi\frac{\langle\varepsilon\rangle^i2}{\langle k\rangle^i} \tag{4}$$

where

$$-\rho\phi\langle\overline{\mathbf{u}'\mathbf{u}'}\rangle^i=\mu_{t_\phi}2\langle\overline{\mathbf{D}}\rangle^v-\frac{2}{3}\phi\rho\langle k\rangle^i\mathbf{I} \tag{5}$$

and

$$\mu_{t_\phi}=\rho c_\mu\frac{\langle k\rangle^{i2}}{\langle\varepsilon\rangle^i} \tag{6}$$

Details on the derivation of the above equations can be found in [17].

2.3. Macroscopic energy equations

Macroscopic energy equations are obtained for both fluid and solid phases by also applying time and volume average operators to the instantaneous local equations [24]. As in the flow case, volume integration is performed over a Representative Elementary Volume (REV). After including the heat released due to the combustion reaction, one gets for both phases:

$$Gas:(\rho c_p)_f\nabla\cdot(\mathbf{u}_D\langle\overline{T}_f\rangle^i)=\nabla\cdot\{\mathbf{K}_{eff,f}\cdot\nabla\langle\overline{T}_f\rangle^i\}+h_ia_i(\langle\overline{T}_s\rangle^i-\langle\overline{T}_f\rangle^i)+\phi\Delta HS_{fu}, \tag{7}$$

$$Solid:0=\nabla\cdot\{\mathbf{K}_{eff,s}\cdot\nabla\langle\overline{T}_s\rangle^i\}-h_ia_i(\langle\overline{T}_s\rangle^i-\langle\overline{T}_f\rangle^i), \tag{8}$$

where, $a_i=A_i/\Delta V$ is the interfacial area per unit volume, h_i is the film coefficient for interfacial transport, $\mathbf{K}_{eff,f}$ and $\mathbf{K}_{eff,s}$ are the effective conductivity tensors for fluid and solid, respectively, given by,

$$\mathbf{K}_{eff,f}=\left\{\overbrace{\phi k_f}^{\text{conduction}}\right\}\mathbf{I}+\underbrace{\mathbf{K}_{f,s}}_{\text{local conduction}}+\underbrace{\mathbf{K}_{disp}}_{\text{dispersion}}+\underbrace{\mathbf{K}_t+\mathbf{K}_{disp,t}}_{\text{turbulence}} \tag{9}$$

$$\mathbf{K}_{\mathrm{eff,s}} = \left\{ \overbrace{(1-\phi)[k_s}^{\text{conduction}} + \frac{\overbrace{16\sigma(\langle \overline{T} \rangle^i)^3}^{\text{radiation}}}{3\beta_r}] \right\} \mathbf{I} + \underbrace{\mathbf{K}_{s,f}}_{\text{local conduction.}} \tag{10}$$

In Eqs. (7)–(10), $\mathbf{I}$ is the unit tensor, ΔH is the heat of combustion [5×10^7 J/kg], β_r is the extinction coefficient [1000 m^{-1}], σ is the Stephan–Boltzman constant [5.66961×10^{-8} W/m^2K^4] and S_{fu} is the rate of fuel consumption, to be commented below. All mechanisms contributing to heat transfer within the medium, together with turbulence and radiation, are included in order to compare their effect on temperature distribution. Further, such distinct contributions of various mechanisms are the outcome of the application of gradient type diffusion models, in the form (see [24] for details).

$$\textit{Turbulent heat flux}: -(\rho c_p)_f \left(\phi \, \overline{\langle \mathbf{u}' \rangle^i \langle T_f' \rangle^i} \right) = \mathbf{K}_t \cdot \nabla \langle \overline{T}_f \rangle^i. \tag{11}$$

$$\textit{Thermal dispersion}: -(\rho c_p)_f \left(\phi \langle \overline{\mathbf{u}}^i \overline{T}_f \rangle^i \right) = \mathbf{K}_{disp} \cdot \nabla \langle \overline{T}_f \rangle^i. \tag{12}$$

$$\textit{Turbulent thermal dispersion}: -(\rho c_p)_f \left(\phi \overline{\langle \mathbf{u}'^i T_f'^i \rangle} \right) = \mathbf{K}_{disp,t} \cdot \nabla \langle \overline{T}_f \rangle^i. \tag{13}$$

$$\textit{Local conduction}: \quad \nabla \cdot \left[\frac{1}{\Delta V} \int_{A_i} \mathbf{n}_i k_f \overline{T}_f dA \right] = \mathbf{K}_{f,s} \cdot \nabla \langle \overline{T}_s \rangle^i \tag{14}$$

$$\nabla \cdot \left[\frac{1}{\Delta V} \int_{A_i} \mathbf{n}_i k_s \overline{T}_s dA \right] = \mathbf{K}_{s,f} \cdot \nabla \langle \overline{T}_f \rangle^i.$$

In Eqs. (7) and (8) the heat transferred between the two phases was modeled by means of a film coefficient h_i. A numerical correlation for the interfacial convective heat transfer coefficient was proposed by Kuwahara et al. [25] for laminar flow as:

$$\frac{h_i D}{k_f} = \left(1 + \frac{4(1-\phi)}{\phi} \right) + \frac{1}{2}(1-\phi)^{1/2} \mathrm{Re}_D \mathrm{Pr}^{1/3}, \text{ valid for } 0.2<\phi<0.9, \tag{15}$$

For turbulent flow, the following expression was proposed in Saito and de Lemos [24]:

$$\frac{h_i D}{k_f} = 0.08 \left(\frac{\mathrm{Re}_D}{\phi} \right)^{0.8} \mathrm{Pr}^{1/3}; \text{ for } 1.0x10^4 < \frac{\mathrm{Re}_D}{\phi} < 2.0x10^7, \text{ valid for } 0.2<\phi<0.9, \tag{16}$$

2.4. Macroscopic mass transport

Transport equation for the fuel reads,

$$\nabla \cdot (\overline{\mathbf{u}}_D \langle \overline{m}_{fu} \rangle^i) = \nabla \cdot \mathbf{D}_{eff} \cdot \nabla (\phi \langle \overline{m}_{fu} \rangle^i) - S_{fu} \tag{17}$$

where $\langle \overline{m}_{fu} \rangle^i$ is the mass fraction for the fuel. The effective mass transport tensor, $\mathbf{D}_{eff}$, is defined as:

$$\mathbf{D}_{eff} = \underbrace{\mathbf{D}_{disp}}_{\text{dispersion}} + \overbrace{\mathbf{D}_{diff}}^{\text{diffusion}} + \underbrace{\mathbf{D}_t + \mathbf{D}_{disp,t}}_{\text{turbulence}} = \mathbf{D}_{disp} + \frac{1}{\rho}\left(\frac{\mu_\phi}{Sc_\ell} + \frac{\mu_{t_\phi}}{Sc_{\ell,t}} \right) \mathbf{I}$$

$$= \mathbf{D}_{disp} + \frac{1}{\rho} \left(\frac{\mu_{\phi,ef}}{Sc_{\ell,ef}} \right) \mathbf{I} \tag{18}$$

where Sc_ℓ and $Sc_{\ell,t}$ are the laminar and turbulent Schmidt numbers for species ℓ, respectively, and the subscript "ef" denotes an effective value. The dispersion tensor is defined such that,

$$-\rho \langle \overline{\mathbf{u}}^i \overline{m}_{fu} \rangle^i = \rho \mathbf{D}_{disp} \nabla \cdot \langle \overline{m}_{fu} \rangle^i \tag{19}$$

2.5. Simple combustion model

In this work, for simplicity, the chemical exothermic reaction is assumed to be instantaneous and to occur in a single step, which is given by the chemical reaction,

$$CH_4 + 2(1+\Psi)(O_2 + 3.76N_2) \rightarrow CO_2 + 2H_2O + 2\Psi O_2 + 7.52(1+\Psi)N_2 \tag{20}$$

where Ψ is the excess air in the reactant stream at the inlet of the porous foam. For the stoichiometric ratio, $\Psi = 0$.

The rate of fuel consumption over the total volume (gas plus solid) was determined by a one step Arrhenious reaction [26] given by

$$S_{fu} = \rho^2 A \langle \overline{m}_{fu} \rangle^i \langle \overline{m}_{ox} \rangle^i \exp[-E / R \langle \overline{T} \rangle^i] \tag{21}$$

where $\langle \overline{m}_{fu} \rangle^i$ and $\langle \overline{m}_{ox} \rangle^i$ are the volume–time averaged mass fractions for the fuel and oxidant, respectively, A is the pre-exponential factor [1×10^{10} m^3/(kg s)] and E is the activation energy [1.4×10^8 J/kmol], where all values used are the ones commonly used in the literature for combustion of methane.

Density ρ in the above equations is determined from the perfect gas equation for a mixture of perfect gases:

$$\rho = \frac{P_o}{R T_f \sum_1^{\ell} \frac{m_\ell}{M_\ell}} \tag{22}$$

where P_o is the absolute pressure, R is the universal gas constant [8.134 J/(mol K)] and M_ℓ is the molecular weight of species ℓ.

2.6. Boundary conditions and numerical details

The set of equations above where solved, for one-dimensional cases, with given temperatures (solid and gas) and fuel mass fraction at inlet, $x = 0$. At exit, $x = 12$ cm, a zero diffusion condition $\partial(\,)/\partial x = 0$ for the fuel mass fraction and gas temperature was used. For the solid temperature, a balance between the energy conducted to the exit and the radiation leaving to the environment was applied. Further, an initial length of 2 cm was considered to be made of a material that prevents flash back of the flame, which is commonly referred to in the literature as "flame trap" [27]. Ignition, is existing, was then calculated for $x > 2$ cm.

3. Results and discussion

The computational grid was generated with a concentration of points close to the beginning of the combustion section ($x > 2$ cm), where steep temperature and species gradients were expected to appear. Two grids were employed with 120 and 240 nodes in the x direction, respectively. Fig. 1 shows temperature profiles calculated with both mentioned grids and indicates that no detectable differences exist between the two sets of results. For this reason, all simulations in this work make use of the 120 node stretched grid.

Fig. 2a shows the effect of excess air Ψ on the gas temperature, T_f, and solid temperature, T_p. Temperature levels for the stoichiometric case and for $\Psi = 0.8$ gave numerical values close to those from [28]. Likewise, mass fraction behavior of species CH_4, CO_2 (Fig. 2b) and H_2O, O_2 (Fig. 2c) follows closely those reported by [28], for the one-

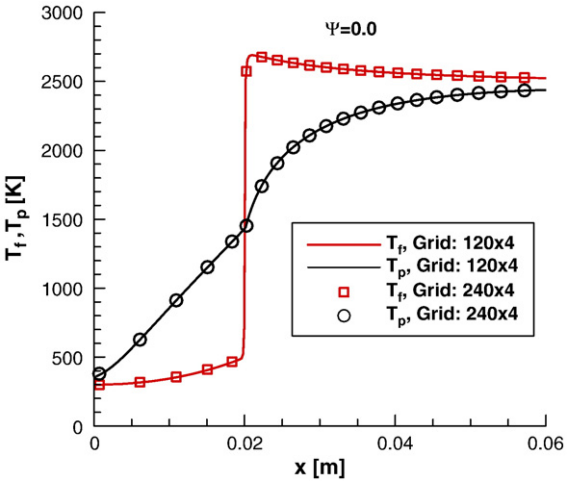

Fig. 1. Grid independence studies.

equation simple combustion model here presented. Excess air reduces the final mass fraction of CO_2 and water and raises the amount of oxygen not participating in the combustion reaction. These results are the outcome of the single step reaction (Eq. (20)) that links the consumption and production rates of individual constituents of the mixture.

Fig. 3 shows the dependence of temperature levels on inlet velocities U_{in}. As axial flow in increased, one can note a slight reduction of peak values of temperatures, followed by the movement of the flame towards the exit of the burner. Although the movement of the flame front is in accordance with simulations by [29], here a reduction on the maximum values of temperatures was calculated, which is in disagreement with findings in the literature [29] where the temperature rises as the inlet mass flow rate is increased. One possible explanation for this contrary behavior is that there are a number of distinct parameters and assumptions in both calculations sets, here and in [29], spanning from mathematical to numerical modeling hypotheses, which might affect the final results.

Four different thermo-mechanical models are now compared, namely Laminar, Laminar with Radiation Transport, Turbulent, Turbulent with Radiation Transport. Radiation model is included by considering the radiation transport term in the T_p—Eq. (10). Turbulence modeling is handled by resolving the k–ε model (Eqs. (3) and (4)) in addition to solving for the macroscopic turbulent eddy viscosity μ_{t_ϕ}, Eq. (6). In all models, combustion is simulated via a unique simple closure, which is presented by Eqs. (20) and (21).

Numerical simulations obtained with different models are presented in Fig. 4 for two values of U_{in}. First, it it interesting to point out that the four models above were used when calculating both inlet velocity values. Therefore, turbulent transport was also considered for low speed flows and that was done in order to verify the correctness and stability of the developed code. In low speed flows, levels of turbulent kinetic energy, if initially input at inlet, will decay and remain low even if a turbulence model is applied. That was the case for $U_{in} = 0.1$ m/s when the pore Reynolds number is of the order of 35. On the order hand, for $U_{in} = 1.0$ m/s, the pore Reynolds number is ten times greater, entering a range where intra-pore turbulence is usually assumed to be significant [17]. With this matter clarified, results can now be presented. Fig. 4a shows that for low value of U_{in}, the flame (solid lines) stabilizes close to the beginning of the burning section ($x = 2$ cm), independently of the mathematical model applied. Also observed in Fig. 4a is that results for the gas temperature are essentially equal when using laminar or turbulence models in low

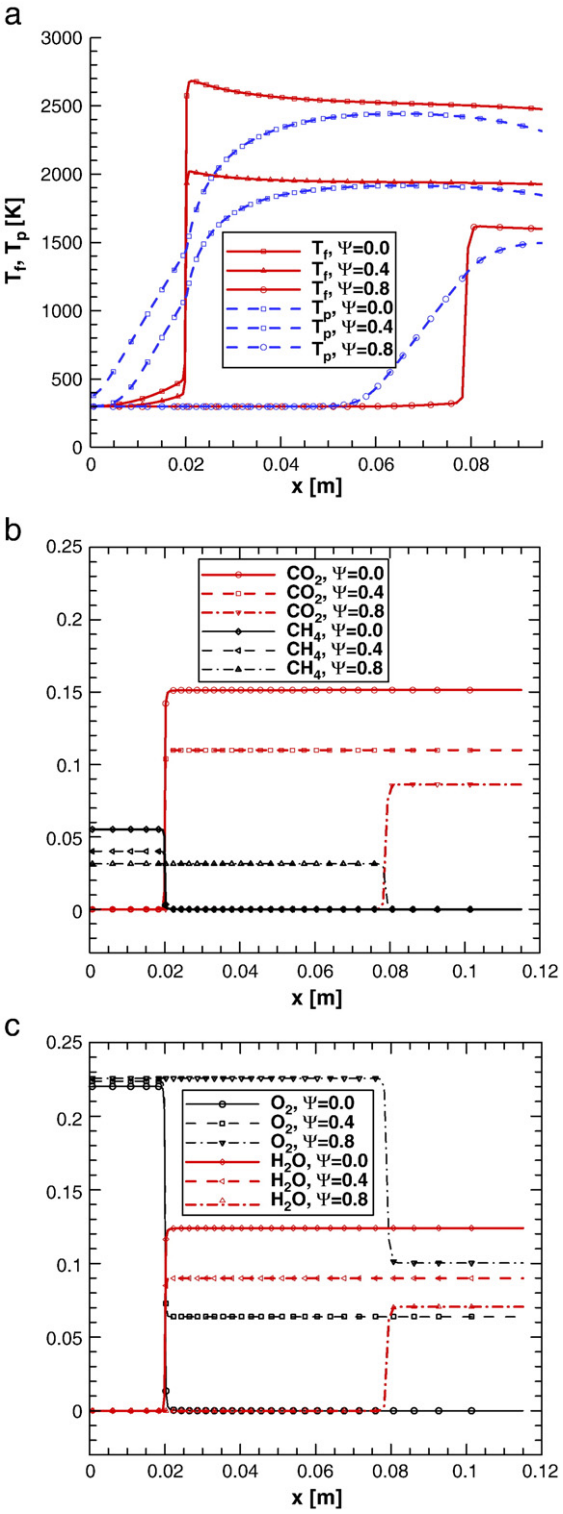

Fig. 2. Effect of excess air Ψ for $U_{in} = 0.1$ m/s on: a) temperature fields, b) fuel and carbon dioxide, c) water and oxygen.

speed cases, which corroborates the observation made above about using a turbulence model in low velocity flows. Solid temperature is influenced by radiation transport, which tends to smooth out temperature differences within the solid matrix, enhancing, as such, the regenerative advantage of porous burners (dashed lines). Regeneration is achieved by preheating the gas prior to the combustion zone. In fact, the use of a turbulence model in conjunction with radiation transport gives the higher temperature peak of the gas

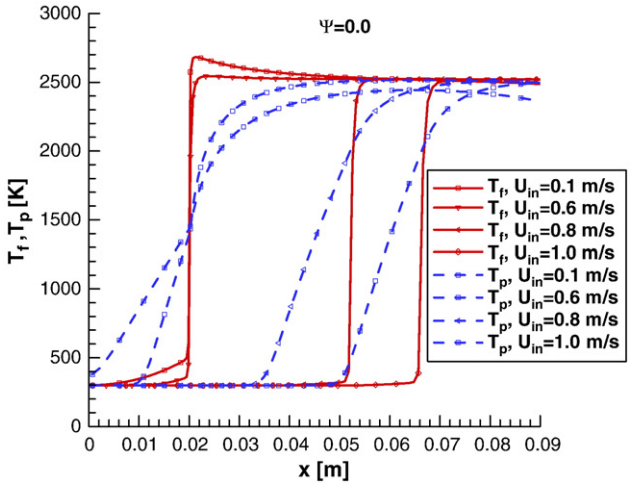

Fig. 3. Effect of inlet gas velocity on temperature fields.

temperature at the flame position. Increasing the inlet mass flow rate (Fig. 4b), the flame is pushed towards the burners' exit, regardless of the model used. In Fig. 4b, no detectable differences in the gas temperature is found when turbulence is the sole mechanism added and compared with the simple laminar model, a result that could be associated with the simple geometry and one-dimensional flow here computed. For multidimensional cases and complex geometries, turbulent transport might play a more significant role. Here also radiation transport substantially affects the solid temperature distribution, but definitive conclusions on the appropriateness of each model can only be reached after careful comparison with experimental measurements. This shall be the subject of the present ongoing research effort.

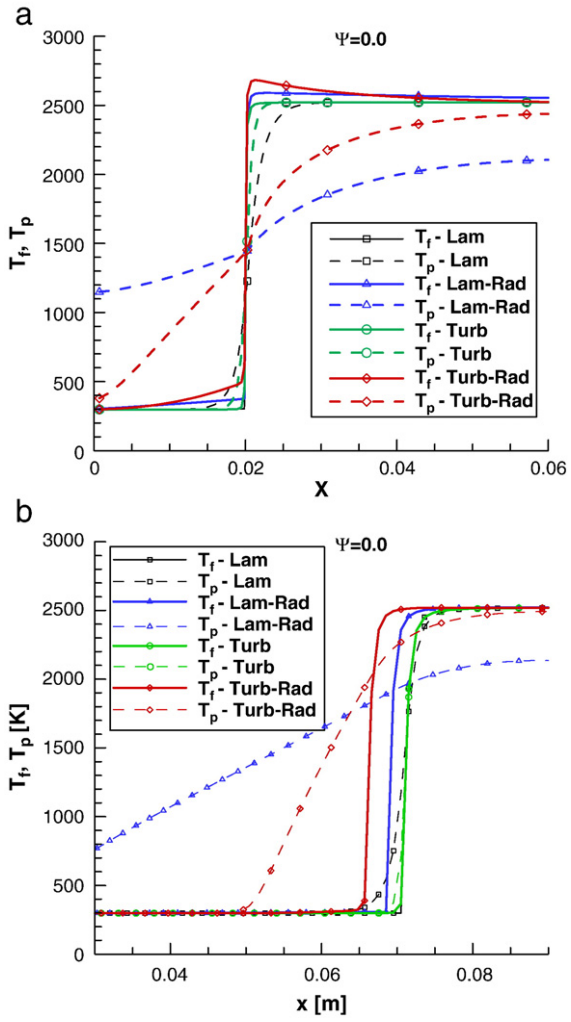

Fig. 4. Comparison of different model solutions: a) $U_{in} = 0.1$ m/s, b) $U_{in} = 1.0$ m/s.

4. Conclusions

This paper presented one-dimensional simulations for combustion of a mixture of air and methane burning in a porous material. Four different thermo-mechanical models were compared along with a unique simple closure for combustion. Results indicate that a substantially different temperature distribution pattern is obtained depending on the model used. For high excess air or gas velocity, the flame front moves towards the exit of the burner. Results herein motivates further research work on the subject of reactive turbulent flow in porous burners and should be seen as a preliminary step towards reliable simulation of multidimensional flow in real porous combustors.

Acknowledgments

The author is indebted to CNPq, CAPES and FAPESP, research funding agencies in Brazil, for their invaluable support during the course of this research endeavor.

References

[1] J.R. Howell, M.J. Hall, J.L. Ellzey, Combustion of hydrocarbon fuels within porous inert media, Progress in Energy and Combustion Science 22 (2) (1996) 121–145.
[2] A.A.M. Oliveira, M. Kaviany, Non Equilibrium in the Transport of Heat and Reactants in Combustion in Porous Media, Progress in Energy and Combustion Science 27 (5) (2001) 523–545.
[3] M.R. Henneke, J.L. Ellzey, Modeling of filtration combustion in a packed bed, Combustion and Flame 117 (4) (1999) 832–840.
[4] P.H. Bouma, L.P.H. De Goey, Premixed combustion on ceramic foam burners, Combustion and Flame 119 (1–2) (Oct 1999) 133–143.
[5] Vs. Babkin, Filtrational combustion of gases—present state of affairs and prospects, Pure and Applied Chemistry 65 (2) (Feb 1993) 335–344.
[6] S.A. Leonardi, R. Viskanta, J.P. Gore, Analytical and experimental study of combustion and heat transfer in submerged flame metal fiber burners/heaters, Journal of Heat Transfer 125 (1) (Feb 2003) 118–125.
[7] F.A. Lammers, L.P.H. De Goey, A numerical study of flash back of laminar premixed flames in ceramic-foam surface burners, Combustion and Flame 133 (1–2) (2003) 47–61.
[8] A.A. Mohamad, S. Ramadhyani, R. Viskanta, Modeling of combustion and heat-transfer in a packed-bed with embedded coolant tubes, International Journal of Heat and Mass Transfer 37 (8) (1994) 1181–1191.
[9] S. Wood, A.T. Harries, Porous burners for lean-burn applications, Progress in Energy and Combustion Science 34 (2008) 667–684.
[10] P.-F. Hsu, J.R. Howell, R.D. Matthews, A numerical investigation of premixed combustion within porous inert media, Journal of Heat Transfer 115 (1993) 744–750.
[11] T.E. Peard, J.E. Peters, Brewster, R.O. Buckius, Radiative heat transfer augmentation in gas-fired radiant tube burner by porous inserts: effect on insert geometry, Experimental Heat Transfer 6 (1993) 273–286.
[12] I.-G. Lim, R.D. Matthews, Development of a Model for Turbulent Combustion Within Porous Inert Media, Trensp. Phenm. Therm. Eng, Begell House Inc. Publ, 1993, pp. 631–636.
[13] W.P. Jones, B.E. Launder, The prediction of laminarization with two-equation model of turbulence, International Journal of Heat and Mass Transfer 15 (1972) 301–314.
[14] M. Sahraoui, L Kaviany, Direct simulation vs time-averaged treatment of adiabatic, premixed flame in a porous medium, International Journal of Heat and Mass Transfer 18 (1995) 2817–2834.
[15] M.J.S. de Lemos, R.A. Silva, Turbulent flow over a layer of a highly permeable medium simulated with a diffusion-jump model for the interface, International Journal of Heat and Mass Transfer 49 (3–4) (2006) 546–556.
[16] M.H.J. Pedras, M.J.S. de Lemos, Computation of turbulent flow in porous media using a low-Reynolds *k*–epsilon model and an infinite array of transversally displaced elliptic rods, Numerical Heat Transfer Part A-Applications 43 (6) (2003) 585–602.

[17] M.J.S. de Lemos, Turbulence in Porous Media: Modeling and Applications, Elsevier, Amsterdam0-08-044491-1, 2006 384 pgs.
[18] N.B. Santos, M.J.S. de Lemos, Flow and heat transfer in a parallel-plate channel with porous and solid baffles, Numerical Heat Transfer Part A-Applications 49 (5) (2006) 471–494.
[19] M. Assato, M.H.J. Pedras, M.J.S. de Lemos, Numerical solution of turbulent channel flow past a backward-facing step with a porous insert using linear and nonlinear *k*–epsilon models, Journal of Porous Media 8 (1) (2005) 13–29.
[20] E.J. Braga, M.J.S. de Lemos, Turbulent natural convection in a porous square cavity computed with a macroscopic kappa–epsilon model, International Journal of Heat and Mass Transfer 47 (26) (2004) 5639–5650.
[21] J.C. Slattery, Flow of viscoelastic fluids through porous media, AIChE J. 13 (1967) 1066–1071.
[22] S. Whitaker, Advances in theory of fluid motion in porous media, Industrial and Engineering Chemistry 61 (1969) 14–28.
[23] W.G. Gray, P.C.Y. Lee, On the theorems for local volume averaging of multiphase system, International Journal of Multiphase Flow 3 (1977) 333–340.
[24] M.B. Saito, M.J.S. de Lemos, A correlation for interfacial heat transfer coefficient for turbulent flow over an array of square rods, Journal of Heat Transfer 128 (2006) 444–452.
[25] F. Kuwahara, M. Shirota, A. Nakayama, A numerical study of interfacial convective heat transfer coefficient in two-energy equation model for convection in porous media, International Journal of Heat and Mass Transfer 44 (2001) 1153–1159.
[26] K.K. Kwo, Principles of Combustion, John Wiley & Sons, New York, 1986.
[27] D. Trimis, F. Durst, Combustion in a porous medium — advances and applications, Combustion Science and Technology 121 (1996) 153–168.
[28] X.Y. Zhou, JCF Pereira Comparison of four combustion models for simulating the premixed combustion in inert porous media, Fire and Materials 22 (1998) 187–197.
[29] A.A. Mohamad, Axial and Radial Porous Burners, Chap 24 in Emerging Technologies and Techniques in Porous Media, Derek B. Ingham, Eden Mamut, Adrian Bejan, Ian Pop (Eds), Springer, Berlin (2004).